

DisReserv (v1.0): Analytical displacement solution due to reservoir compaction with arbitrary geometry and under arbitrary pressure changes

Valeria C. F. Barbosa¹, Vanderlei C. Oliveira Jr.¹, and Andre D. Arelaro^{1,2}

¹Department of Geophysics, Observatório Nacional, Rio de Janeiro, Brazil

²PETROBRAS, Rio de Janeiro, Brazil

Correspondence: Valeria C. F. Barbosa (valcris@on.br)

Abstract. We have presented analytical solutions for the displacement due to reservoir compaction with arbitrary geometry and under arbitrary pressure changes. These solutions are based on the similarity between the gravitational potential yielded by a volume source under a density variation and the displacement field yielded by a volume source in a half-space under a pressure variation. This similarity enables the use of closed expressions of the gravitational potential and its derivatives for calculating the displacement field due to a volume source under a pressure variation. We discretized the reservoir as a grid of 3D right rectangular prisms juxtaposed in the horizontal and vertical directions. Each prism has homogeneous pressure; however, pressure variations among different prisms are allowed. This parametrization of the reservoir yields a piecewise-constant distribution of pressure in the subsurface. The discrete reservoir modeling to calculate the displacement field due to this pressure variation follows the nucleus-of-strain concept in which the center of each prism represents the coordinate of a nucleus of strain. The displacement due to a nucleus of strain is considered the infinitesimal element of the displacement due to an infinitesimal reservoir. The displacement field due to the pressure of each prism is calculated by integrating the infinitesimal element of the displacement over the volume of the prism. Finally, the displacement due to the reservoir can be approximated by the sum of the contributions of each prism of the discretized model. We provide python codes (DisReserv) to calculate the displacement fields due to a reservoir with arbitrary shape and distribution of pressure changes. The displacement field is calculated inside and outside the reservoir. We calculate the displacement fields in three scenarios: i) cylindrical reservoir under uniform depletion; ii) cylindrical reservoir under non uniform depletion and iii) reservoir with arbitrary geometry and under arbitrary pressure distribution. By calculating the stress field at the free surface, we verify that the zero stress condition is satisfied.

Copyright statement.

20 **1 Introduction**

The surface subsidence due to oil or gas withdrawal from a reservoir in the subsurface may occur as a result of geomechanical changes caused by pressure drop. The phenomenon of subsidence by fluid extraction has been observed in a variety of oil fields, e.g., the Ekofisk field, southern North Sea (Borges et al., 2020) and the Groningen gas field in the northeast Netherlands (van Thienen-visser and Fokker, 2017). Because the subsidence close to hydrocarbon fields under production can induce earthquakes
25 (e.g., Dahm et al., 2015; Grigoli et al., 2017), the petroleum companies have been an increased interest in monitoring the magnitude and distribution of subsidence resulting from reservoir depletion. The subsidence monitoring is accomplished by means of calculating the displacement field for a given set of reservoir properties.

The possibility of occurrence of catastrophic events, related to subsidence due to extraction or injection of fluids in reservoir, has stimulated efforts to develop analytical methods for modeling the displacement and stress fields due to reservoir compactation.
30 The physical foundation of the displacement, stress and strain fields in the subsurface due to a reduction of pressure in the reservoir comes from the theory of thermoelasticity. Theory of thermoelasticity has been laid in the first half of the nineteenth century to describe the interaction between the thermal field and elastic bodies. In the uncoupled thermoelasticity theory for quasi-static problems (i.e., problems with negligible inertia effects), Goodier (1937) employed the method of superposition using displacement potential functions and introduced the concept of nucleus of thermoelastic strain in an infinite space.
35 Specifically, Goodier's (1937) method simplified the thermoelastic problem by replacing it by an isothermal elastic problem with different boundary conditions together with the solution of a Poisson's equation (Tao, 1971). Mindlin and Cheng (1950) and Sen (1951) extended the Goodier's method to a homogenous half-space. Sharma (1956) deduced the displacement and stress fields in an infinite elastic plate due to a nucleus of thermoelastic strain located at a point inside it by using infinite integrals involving Bessel functions.

40 The subsidence resulting from reservoir depletion is in the context of poroelastic theory. Geertsma (1957) remarked the analogy between the theories of thermoelasticity and poroelasticity. To our knowledge, Geertsma (1973) was the first to solve the poroelastic problem by using the nucleus-of-strain concept in the half-space, which in turn was proposed by Mindlin and Cheng (1950) and Sen (1951) in the theory of thermoelasticity. Geertsma (1973) derived analytical expressions for the stress and displacement fields for a thin disk-shaped reservoir. Segall (1992) followed Geertsma (1973) and extended the analytical
45 solutions of the displacement and stress fields assuming general axisymmetric geometries and an arbitrary radial pressure distribution.

Geertsma and van Opstal (1973) applied the nucleus-of-strain concept in the half-space to calculate the spatial subsidence distribution due to the production of reservoir with an arbitrary 3D shape. By assuming a producing reservoir embedded in an a homogeneous, isotropic, and elastic medium, and a reservoir model in which the pressure perturbations are related to the
50 displacement field by a linear relationship, Geertsma and van Opstal (1973) discretized the reservoir into a grid of prisms and calculated the displacement due to the pressure change in the whole reservoir by the superposition of the displacement due to the constant pressure change in each prism. Tempone et al. (2010) adopted the same reservoir model used in Geertsma and van Opstal (1973) and extended the nucleus-of-strain concept in the half-space to consider the effects of a rigid basement. Similarly,

Tempone et al. (2010) assumed a reservoir embedded in an a homogeneous, isotropic, and elastic medium and calculated the displacement, stress and strain fields subject to uniform depletion. The main drawbacks in Geertsma and van Opstal (1973) and Tempone et al. (2010) are the assumption of homogeneous reservoir and the solution is only valid outside the reservoir. In this case, the displacements within the reservoir are calculated by a linear interpolation of the displacements at the upper and lower edges of the reservoir (Tempone et al., 2012).

Considering an inhomogeneous poroelastic model consists of layered stratigraphy, Mehrabian and Abousleiman (2015) developed closed-form formulae for the displacement and stress fields outside and inside of the reservoir embedded within elastic strata with different mechanical properties and subjected to pore pressure disturbances due to fluid extraction or injection. By assuming a linear elastic semi-infinite medium, Muñoz and Roehl (2017) developed analytical solution for the displacement field outside and inside of an arbitrarily-shaped reservoir under arbitrary distribution of pressure changes. Muñoz and Roehl (2017) parametrized the reservoir into a grid of 3D prisms and used the nucleus-of-strain concept. The nucleus of strain is taking as an infinitesimal volume element for each prism and the displacement solution due to each prism is obtained by a three-dimensional integration over the prism volume. The displacement field outside and inside of the reservoir is given by the summation of the displacement fields of the displacements produced by all prisms setting up the reservoir model.

The present work assumes a linear elastic semi-infinite medium and provides an analytical solution for displacement field due to an arbitrarily-shaped reservoir under arbitrary distribution of pressure changes. Like Muñoz and Roehl (2017) we used the nucleus-of-strain concept and discretized the reservoir into a grid of 3D prisms along the x -, y - and $-z$ directions. We also consider the nucleus of strain as an infinitesimal volume element for each prism and the displacement solution due to each prism is obtained by a three-dimensional integration over the prism volume. The final displacement field due to the whole reservoir is the sum of the displacements produced by the prisms. In contrast with Muñoz and Roehl (2017)'s method we take advantage the similarity between the equations for calculating the displacement field due to a volume source in a half-space under a pressure variation and the gravitational potential due to a volume source under a density variation. This similarity makes possible the use of closed expressions of the gravitational potential and its derivatives produced by the 3D right rectangular prism derived by Nagy et al. (2000) and (2002) and Fukushima (2020) for calculating the displacement field due to a volume source under a pressure variation. The adopted exact analytical formulae of the gravitational field are valid expressions either outside or inside the prisms because the implemented expressions make use of modified arctangent function proposed by Fukushima (2020). We present routines written in Python language (Python 3.7.6) to calculate the displacement fields due to a reservoir with arbitrary shape and distribution of pressure changes. We validate our equations by verifying that at the free surface the stress fields are null. Tests with synthetic data validate our approach.

2 THEORY

The subsidence or displacement, stress and strain fields in the subsurface caused by reservoir compaction due to hydrocarbon production are grounded on the theory of thermoelasticity.

The Goodier's thermoelastic displacement potential ϕ satisfies the Poisson's equation (Goodier, 1937), i.e.:

$$\nabla^2 \phi = m T, \quad (1)$$

where ∇^2 is the Laplacian operator, T is the temperature difference and

$$m = \alpha \frac{1+\nu}{1-\nu}, \quad (2)$$

90 where α is the coefficient of linear thermal expansion and ν is the Poisson's ratio.

From the potential theory, a particular solution of equation 1 is

$$\phi(x, y, z) = -\frac{m}{4\pi} \int_v \int \int \frac{T(x', y', z')}{\sqrt{(x-x')^2 + (y-y')^2 + (z-z')^2}} dv, \quad (3)$$

where $\phi(x, y, z)$ represents the Newtonian gravitational potential (Kellogg, 1929) at the coordinates x, y and z produced by a continuous distribution of mass defined by a set of very small masses $-\frac{m}{4\pi} T(x', y', z') dv$, where $T(x', y', z')$ stands for the density distribution. The integral in equation 3 is conducted over the coordinates x', y' and z' , denoting, respectively, the x -, y - and $-z$ coordinates of an arbitrary point belonging to the interior of the volume v of the gravity source.

From equation 3 and the potential-field theory, Goodier (1937) showed that if an element of volume dv in the infinite solid is at a temperature $T(x', y', z')$, the remainder being at temperature zero, the displacement vector \mathbf{u} caused by this temperature is the gradient of the Goodier's thermoelastic displacement potential, i.e.,

$$100 \quad \mathbf{u} = \nabla \phi(x, y, z). \quad (4)$$

where ∇ is the gradient operator.

To a homogenous half-space, Mindlin and Cheng (1950) showed that the method proposed by Goodier (1937) can be extended by the displacement solution given by:

$$\mathbf{u} = \nabla \phi_1 + \nabla_2 \phi_2, \quad (5)$$

105 where $\phi_1 \equiv \phi_1(x, y, z)$ is the potential defined in equation 3, $\phi_2 \equiv \phi_2(x, y, z)$ is defined as "image potential" (Segall, 1992) due to a image point at the coordinates $(x', y', -z')$ and the operator ∇_2 is expressed by

$$\nabla_2 = (3-4\nu)\nabla + 2\nabla_z \frac{\partial}{\partial z} - 4(1-\nu)\hat{\mathbf{z}}\nabla_z^2, \quad (6)$$

where $\hat{\mathbf{z}}$ is the unit vector in the z -direction and ∇_z^2 is a scalar operator in which the operand is firtly multiplied by z and then operated upon by Laplacian operator ∇^2 .

110 Equation 5 is the displacement solution for the variation of temperature due to a single nucleus of strain buried at depth z' in a semi-infinite homogeneous medium. In the right hand side of equation 5, the first term $\nabla \phi_1$ represents the displacement in an infinite medium, and the second term represents a correction of the displacement due a half-space, also known as image nucleus solution.

3 METHODOLOGY

115 Let's assume that a reservoir in the interior of the Earth is subject to a compaction due to hydrocarbon production. The compaction is caused by the pressure change within the reservoir, which in turn causes a surface subsidence (or surface displacement). We discretized the reservoir into an $m_x \times m_y \times m_z$ grid of 3D vertical juxtaposed prisms ($m_x \cdot m_y \cdot m_z = M$) in which the pressure within each prism is assumed to be constant and known. Each grid prism in the reservoir model may undergo a distinct pressure change. Hence, the subsidence effect is the displacement field due to the pressure change throughout
120 the reservoir and it can be calculated by the sum of the displacement produced by each prism.

The discrete forward modeling to calculate the displacement and stress fields due to a piecewise-constant distribution of the pressure contrast within a reservoir follows the nucleus of strain approach. By assuming that the center of each prism represents the coordinate of a nucleus of strain, we can calculate the displacement field due to the pressure contrast of this prism by integrating over its volume. The displacement solution for a single nucleus of strain in a homogeneous elastic semi-infinite medium (equation 5) will be used as an element of the displacement.
125

3.1 The discrete forward modeling due to a nucleus of strain in a homogeneous elastic semi-infinite medium

Here, we use a Cartesian coordinate system with the x -axis pointing to north, the y -axis pointing to east and the z -axis pointing downward. By considering the discrete form of equation 5, the displacement field $\mathbf{u}_i \equiv \mathbf{u}(x_i, y_i, z_i)$ at an arbitrary point (x_i, y_i, z_i) due to the j th nucleus of strain at the coordinates (x'_j, y'_j, z'_j) will be calculated by

$$130 \quad \mathbf{u}_i = \nabla \phi_1(x_i, y_i, z_i, x'_j, y'_j, z'_j) + \nabla_2 \phi_2(x_i, y_i, z_i, x'_j, y'_j, z'_j), \quad (7)$$

In equation 7, the functions $\phi_1 \equiv \phi_1(x_i, y_i, z_i, x'_j, y'_j, z'_j)$ and $\phi_2 \equiv \phi_2(x_i, y_i, z_i, x'_j, y'_j, -z'_j)$ are, respectively, given by

$$\phi_1 = -\frac{C_m}{4\pi} \frac{\Delta p_j \ dv_j}{R_{1ij}} \quad (8)$$

and

$$\phi_2 = -\frac{C_m}{4\pi} \frac{\Delta p_j \ dv_j}{R_{2ij}}. \quad (9)$$

135 In equations 8 and 9, Δp_j is the pressure contrast of the j th nucleus, dv_j is an infinitesimal element of volume of the j th nucleus, and C_m is the uniaxial compaction coefficient (see Geertsma, 1966; Tempone et al., 2010 and Muñoz and Roehl, 2017) given by

$$C_m = \frac{1}{E} \frac{(1+\nu)(1-2\nu)}{(1-\nu)}, \quad (10)$$

where E is the Young's modulus.

140 In equation 8, R_{1ij} is the distance from the i th coordinate point of the displacement (x_i, y_i, z_i) to the j th coordinate of the nucleus of strain (x'_j, y'_j, z'_j) , i.e.:

$$R_{1ij} = \sqrt{(x_i - x'_j)^2 + (y_i - y'_j)^2 + (z_i - z'_j)^2}. \quad (11)$$

In equation 9, R_{2ij} is the distance from the i th coordinate point of the displacement (x_i, y_i, z_i) to the j th coordinate of the image nucleus $(x'_j, y'_j, -z'_j)$, i.e.:

$$145 \quad R_{2ij} = \sqrt{(x_i - x'_j)^2 + (y_i - y'_j)^2 + (z_i + z'_j)^2}. \quad (12)$$

Figure 1 shows a schematic representation of the geometry of the nucleus of strain problem in a semi-infinite medium. The j th nucleus of strain is located at the coordinates (x'_j, y'_j, z'_j) . The j th image nucleus is located at the coordinates $(x'_j, y'_j, -z'_j)$. The distances from the i th coordinate point of the displacement (x_i, y_i, z_i) to the j th nucleus of strain and to the j th image nucleus are, respectively, R_{1ij} (equation 11) and R_{2ij} (equation 12). The free surface is a horizontal plane where the components of the stress are null.

Following the discrete form of the displacement solution (equation 7), the displacement field at the coordinates x_i, y_i and z_i due to the j th single nucleus at the coordinates (x'_j, y'_j, z'_j) can be written as:

$$\mathbf{u}_i(x_i, y_i, z_i) = \mathbf{u}_{1i}(x_i, y_i, z_i) + \mathbf{u}_{2i}(x_i, y_i, z_i), \quad (13)$$

where $\mathbf{u}_{1i}(x_i, y_i, z_i) \equiv \mathbf{u}_{1i}$ is the gradient of the function ϕ_1 (equation 8)

$$155 \quad \mathbf{u}_{1i} = \nabla \phi_1(x_i, y_i, z_i, x'_j, y'_j, z'_j) = \frac{A(1+\nu)}{E} \nabla \left(\frac{1}{R_{1ij}} \right) \Delta p_j dv_j \quad (14)$$

and $\mathbf{u}_{2i}(x_i, y_i, z_i) \equiv \mathbf{u}_{2i}$ is obtained by applying the operator ∇_2 (equation 6) to the imagem potential ϕ_2 (equation 9)

$$\mathbf{u}_{2i} = \nabla_2 \phi_2(x_i, y_i, z_i, x'_j, y'_j, -z'_j) = \frac{A(1+\nu)}{E} \left[(3-4\nu) \nabla \left(\frac{1}{R_{2ij}} \right) + 2 \nabla \left(z \frac{\partial}{\partial z} \frac{1}{R_{2ij}} \right) - 4(1-\nu) \hat{\mathbf{z}} \nabla^2 \left(\frac{z}{R_{2ij}} \right) \right] \Delta p_j dv_j, \quad (15)$$

where A is a constant given by:

$$A = -\frac{C_m E}{4\pi(1+\nu)}. \quad (16)$$

160 The elements of the displacement vector \mathbf{u}_{1i} (equation 14) are

$$\mathbf{u}_{1i} = \begin{bmatrix} u_{1x} \\ u_{1y} \\ u_{1z} \end{bmatrix} = \frac{A(1+\nu)}{E} \begin{bmatrix} \frac{\partial}{\partial x} \frac{1}{R_{1ij}} \\ \frac{\partial}{\partial y} \frac{1}{R_{1ij}} \\ \frac{\partial}{\partial z} \frac{1}{R_{1ij}} \end{bmatrix} \Delta p_j dv_j, \quad (17)$$

where u_{1x} , u_{1y} and u_{1z} are the x –, y – and z – components of \mathbf{u}_{1i} that gives the displacement field at the coordinates x_i, y_i and z_i due to the j th single nucleus in the infinite space.

The elements of the displacement vector \mathbf{u}_{2i} (equation 15) are

$$165 \quad \mathbf{u}_{2i} = \begin{bmatrix} u_{2x} \\ u_{2y} \\ u_{2z} \end{bmatrix} = \frac{A(1+\nu)}{E} \left\{ (3-4\nu) \begin{bmatrix} \frac{\partial}{\partial x} \frac{1}{R_{2ij}} \\ \frac{\partial}{\partial y} \frac{1}{R_{2ij}} \\ -\frac{\partial}{\partial z} \frac{1}{R_{2ij}} \end{bmatrix} + 2 z_i \begin{bmatrix} \frac{\partial^2}{\partial x \partial z} \frac{1}{R_{2ij}} \\ \frac{\partial^2}{\partial y \partial z} \frac{1}{R_{2ij}} \\ \frac{\partial^2}{\partial z^2} \frac{1}{R_{2ij}} \end{bmatrix} \right\} \Delta p_j dv_j, \quad (18)$$

where u_{2x} , u_{2y} and u_{2z} are the x –, y – and z – components of \mathbf{u}_{2i} that gives the correction of the displacements considering a semi-space (image nucleus solution).

By following Sharma (1956) and Tempone et al. (2010), the Beltrami's equations (Beltrami, 1902–1920) and the equilibrium equations must be satisfied to obtain the contribution of the stress field in the half space. The stress field at the coordinates x_i ,
170 y_i and z_i due to the j th single nucleus of strain buried in the half space is given by

$$\boldsymbol{\sigma}_i(x_i, y_i, z_i) = \boldsymbol{\sigma}_1(x_i, y_i, z_i) + \boldsymbol{\sigma}_2(x_i, y_i, z_i) \quad (19)$$

where $\boldsymbol{\sigma}_1(x_i, y_i, z_i) \equiv \boldsymbol{\sigma}_{1i}$ represents the stress in an infinite medium, and $\boldsymbol{\sigma}_2(x_i, y_i, z_i) \equiv \boldsymbol{\sigma}_{2i}$ represents a correction of the stress in a half-space due to an image nucleus. Besides the Beltrami's equations (Beltrami, 1902–1920) and the equilibrium equations that must be satisfied, the following boundary conditions at the free surface ($z_i = 0$) must be satisfied, i.e.:

$$175 \quad \boldsymbol{\sigma}_i(x_i, y_i, 0) = \boldsymbol{\sigma}_1(x_i, y_i, 0) + \boldsymbol{\sigma}_2(x_i, y_i, 0) = \mathbf{0}, \quad (20)$$

where $\mathbf{0}$ is the null vector that represents the null stress at the coordinates x_i , y_i and $z_i = 0$.

The elements of the stress vector $\boldsymbol{\sigma}_{1i}$ (equation 19) are

$$\boldsymbol{\sigma}_{1i} = \begin{bmatrix} \widehat{xz}_1 \\ \widehat{yz}_1 \\ \widehat{zz}_1 \end{bmatrix} = A \begin{bmatrix} \frac{\partial^2}{\partial x \partial z} \frac{1}{R_{1ij}} \\ \frac{\partial^2}{\partial y \partial z} \frac{1}{R_{1ij}} \\ \frac{\partial^2}{\partial z^2} \frac{1}{R_{1ij}} \end{bmatrix} \Delta p_j \ dv_j, \quad (21)$$

where \widehat{xz}_1 , \widehat{yz}_1 and \widehat{zz}_1 are the x –, y – and z –components of $\boldsymbol{\sigma}_{1i}$ that gives the stress in an infinite medium due to the j th
180 nucleus of strain.

The elements of the stress vector $\boldsymbol{\sigma}_{2i}$ (equation 19) are

$$\boldsymbol{\sigma}_{2i} = \begin{bmatrix} \widehat{xz}_2 \\ \widehat{yz}_2 \\ \widehat{zz}_2 \end{bmatrix} = A \left\{ \begin{bmatrix} \frac{\partial^2}{\partial x \partial z} \frac{1}{R_{2ij}} \\ \frac{\partial^2}{\partial y \partial z} \frac{1}{R_{2ij}} \\ -\frac{\partial^2}{\partial z^2} \frac{1}{R_{2ij}} \end{bmatrix} + 2 z_i \begin{bmatrix} \frac{\partial^3}{\partial x \partial z^2} \frac{1}{R_{2ij}} \\ \frac{\partial^3}{\partial y \partial z^2} \frac{1}{R_{2ij}} \\ \frac{\partial^3}{\partial z^3} \frac{1}{R_{2ij}} \end{bmatrix} \right\} \Delta p_j \ dv_j, \quad (22)$$

where \widehat{xz}_2 , \widehat{yz}_2 and \widehat{zz}_2 are the x –, y – and z –components of $\boldsymbol{\sigma}_{2i}$ that gives the correction of the stress considering a semi-space due to the j th image nucleus.

185 We validate our equations by verifying if the null stress acting through the free surface (equation 20) is satisfied. Hence, by taking the elements of stress vectors $\boldsymbol{\sigma}_{1i}$ and $\boldsymbol{\sigma}_{2i}$ at the i th coordinates of the free surface (x_i , y_i and $z_i = 0$) the following relationship:

$$\widehat{xz}_1 + \widehat{xz}_2 = \widehat{yz}_1 + \widehat{yz}_2 = \widehat{zz}_1 + \widehat{zz}_2 = 0 \quad (23)$$

must be met.

190 3.2 The discrete displacement forward modeling due to a reservoir in a homogeneous elastic semi-infinite medium

We parameterized the reservoir as a grid of juxtaposed right rectangular prisms. Each grid prism has homogeneous pressure contrasts; however, pressure variations among different prisms are allowed. To calculate the displacement due to the pressure change in the whole reservoir with this discretization model, we use the solution deduced for a single nucleus of strain in a homogeneous elastic semi-infinite medium (subsection 3.1) in the following way. First, we assume that the coordinates of the 195 j th prism center are the coordinates of a nucleus of strain. Next, the displacement field calculated at the i th coordinates (x_i , y_i , z_i) due to the pressure contrast of the j th prism is calculated with a integration over its volume. Then, from equation 13, the displacement field produced by the j th prism can be written as

$$\mathbf{u}_i(x_i, y_i, z_i) = \int_{z_1}^{z_2} \int_{y_1}^{y_2} \int_{x_1}^{x_2} \mathbf{u}_{1i} dx'_j dy'_j dz'_j + \int_{z_1}^{z_2} \int_{y_1}^{y_2} \int_{x_1}^{x_2} \mathbf{u}_{2i} dx'_j dy'_j dz'_j. \quad (24)$$

In equation 24, \mathbf{u}_{1i} is the displacement field at the coordinates x_i , y_i and z_i due to the j th single nucleus in the infinite space 200 (equations 14 and 17), the limits of the integrals represent the borders of the j th prism modeling the reservoir in the following way: x_1 and x_2 are their south and north borders; y_1 and y_2 are their west and east borders; and z_1 and z_2 are their depths to the top and bottom. Additionally, \mathbf{u}_{2i} is the displacement field at the coordinates x_i , y_i and z_i due to the effect of an image nucleus (equations 15 and 18).

Note that the integrations in equation 24, are conducted with respect to the variables (x'_j, y'_j, z'_j) , denoting, respectively, the 205 x –, y –, and z –coordinates of an arbitrary point belonging to the interior of the j th prism (or the j th image nucleus). Finally, the displacement field at the coordinates x_i , y_i and z_i due to the pressure change in the whole reservoir can be defined as the sum of the displacements yielded by each prism with constant pressure Δp_j :

$$\tilde{\mathbf{u}}_i(x_i, y_i, z_i) = \sum_{j=1}^M \int_{z_1}^{z_2} \int_{y_1}^{y_2} \int_{x_1}^{x_2} \mathbf{u}_{1i} dx'_j dy'_j dz'_j + \int_{z_1}^{z_2} \int_{y_1}^{y_2} \int_{x_1}^{x_2} \mathbf{u}_{2i} dx'_j dy'_j dz'_j, \quad (25)$$

where M is the number of prisms setting up the reservoir model.

210 From equation 17, we can get the α –components of the displacement vectors \mathbf{u}_{1i} (the integrand of the first integral of equation 25)

$$u_{1\alpha} = \frac{A(1+\nu)}{E} \left[\frac{\partial}{\partial \alpha} \frac{1}{R_{1ij}} \right] \Delta p_j \quad (26)$$

where α belongs to the set of x – y – and z –directions of the Cartesian coordinates system.

From equation 18, we can get the x – and y –components of the displacement vectors \mathbf{u}_{2i} (the integrand of the second 215 integral of equation 25)

$$u_{2\alpha} = \frac{A(1+\nu)}{E} \left[(3-4\nu) \frac{\partial}{\partial \alpha} \frac{1}{R_{2ij}} + 2 z_i \frac{\partial^2}{\partial \alpha \partial z} \frac{1}{R_{2ij}} \right] \Delta p_j, \quad (27)$$

where α belongs to the set of x - and y -directions, and the z -component of the displacement vectors \mathbf{u}_{2i}

$$u_{2z} = \frac{A(1+\nu)}{E} \left[-(3-4\nu) \frac{\partial}{\partial z} \frac{1}{R_{2ij}} + 2z_i \frac{\partial^2}{\partial z^2} \frac{1}{R_{2ij}} \right] \Delta p_j \quad (28)$$

Equation 26 shows that the α -component of the displacement vector \mathbf{u}_{1i} depends on the first derivative of $\frac{1}{R_{1ij}}$ with respect to the variable α . Conversely, the α -component of the displacement vector \mathbf{u}_{2i} (equation 27) depends not only on the first derivative of $\frac{1}{R_{2ij}}$ with respect to the variable α but also on the second derivative of $\frac{1}{R_{2ij}}$ with respect to the variables α and z .

By substituting equations 26 – 28 into equation 25, we can obtain, respectively, the α -component (where $\alpha = x$ and y) and the z -component of the displacement field at the i th coordinates (x_i , y_i and z_i) due to the pressure change in the whole reservoir, i.e.:

$$225 \quad \tilde{u}_{i\alpha} = \frac{A(1+\nu)}{E} \sum_{j=1}^M \Delta p_j \int_{v_j} \int \int \frac{\partial}{\partial \alpha} \frac{1}{R_{1ij}} dv_j + (3-4\nu) \int_{v_j} \int \int \frac{\partial}{\partial \alpha} \frac{1}{R_{2ij}} dv_j + 2z_i \int_{v_j} \int \int \frac{\partial^2}{\partial \alpha \partial z} \frac{1}{R_{2ij}} dv_j, \quad (29)$$

and

$$\tilde{u}_{iz} = \frac{A(1+\nu)}{E} \sum_{j=1}^M \Delta p_j \int_{v_j} \int \int \frac{\partial}{\partial z} \frac{1}{R_{1ij}} dv_j - (3-4\nu) \int_{v_j} \int \int \frac{\partial}{\partial z} \frac{1}{R_{2ij}} dv_j + 2z_i \int_{v_j} \int \int \frac{\partial^2}{\partial z^2} \frac{1}{R_{2ij}} dv_j, \quad (30)$$

where dv_j is the j th element of volume of the j th prism whose volume is v_j .

In the right-hand side of equations 29 and 30, the three integrals are equal to quantities of the gravitational attraction produced by the j th prism considering that Δp_j is the density of the j th prism and the constants are equivalent to the gravitational constant. The first integral corresponds to the α -component of the gravitational attraction produced by the j th prism. The second and third integrals correspond, respectively, to the α -component of the gravitational attraction and to the αz -component of the gravity gradient tensor produced by the j th image nucleus.

The similarity between the displacement fields due to a volume source in a half-space and the gravity field allows the use of closed expressions of the gravitational potential and its derivatives produced by the 3D right rectangular prism derived by Nagy et al. (2000) and (2002).

The first integral in the right-hand side of equations 29 and 30 is the first derivatives of $\frac{1}{R_{1ij}}$ with respect to x , y and z which are, respectively, given by the following closed expressions:

$$\int_{v_j} \int \int \frac{\partial}{\partial x} \frac{1}{R_{1ij}} dv_j = \left| \left| \left| y \ln(z+R_1) + z \ln(y+R_1) - x \tan^{-1} \left(\frac{yz}{xR_1} \right) \right|^{x_2} \right|^{y_2} \right|^{z_2} \quad (31)$$

240

$$\int_{v_j} \int \int \frac{\partial}{\partial y} \frac{1}{R_{1ij}} dv_j = \left| \left| \left| x \ln(z+R_1) + z \ln(x+R_1) - y \tan^{-1} \left(\frac{xz}{yR_1} \right) \right|^{x_2} \right|^{y_2} \right|^{z_2} \quad (32)$$

$$\int_{v_j} \int \int \frac{\partial}{\partial z} \frac{1}{R_{1ij}} dv_j = \left| \left| \left| x \ln(y+R_1) + y \ln(x+R_1) - z \tan^{-1} \left(\frac{xy}{zR_1} \right) \right|^{x_2} \right|^{y_2} \right|^{z_2} \quad (33)$$

For simplicity, we omit the subscripts i and j in equations 31 – 33; hence, the variables x , y and z are relative coordinates of the
 245 i th point of the displacement referred to the coordinates to the corner of the j th prism modeling the reservoir, i.e., $x = x_j - x_i$,
 $y = y_j - y_i$, $z = z_j - z_i$ and $R_1 = \sqrt{x^2 + y^2 + z^2}$. In equations 31 – 33, the limits of the integrals represent the borders of
 the j th prism modeling the reservoir in the following way: x_1 and x_2 are their south and north borders; y_1 and y_2 are their west
 and east borders; and z_1 and z_2 are their depths to the top and bottom. Nagy et al. (2000) and (2002) provided limit values of
 integrals shown in equations 31 – 33 when the computation point coincides with the corner of the prism.

250 The second and third integrals in the right-hand side of equations 29 and 30 are related with the correction of the displacements
 considering a semi-space (image nucleus solution). These integrals depend on the distance R_{2ij} from the i th coordinate
 point of the displacement to the j th image nucleus. Likewise, $R_2 = \sqrt{x^2 + y^2 + z^2}$; however, the variable z that represents
 the relative coordinate of the i th point of the displacement referred to the coordinates to the corner of the j th image nucleus is
 given by

$$255 \quad z = z_j - z_i - 2z_c \quad (34)$$

where z_c is the z -coordinate of the j th image nucleus

$$z_c = 0.5(z_1 + z_2) \quad (35)$$

The second integral in the right-hand side of equations 29 and 30 is the first derivatives of $\frac{1}{R_{2ij}}$ with respect to x , y and z .
 These derivatives are equal to equations 31 – 33, the only difference is the variable z that is given by equations 34 and 35.

260 The third integral in the right-hand side of equations 29 and 30 is the second derivatives of $\frac{1}{R_{2ij}}$ with respect to xz , yz and
 zz which are, respectively, given by the following closed expressions:

$$\int \int \int_{v_j} \frac{\partial^2}{\partial x \partial z} \frac{1}{R_{2ij}} dv_j = \left| \left| \ln(y + R_2) \right| \right|^{x_2}_{x_1} \left| \left| y_2 \right| \right|^{z_2}_{z_1} \quad (36)$$

$$\int \int \int_{v_j} \frac{\partial^2}{\partial y \partial z} \frac{1}{R_{2ij}} dv_j = \left| \left| \ln(x + R_2) \right| \right|^{x_2}_{x_1} \left| \left| y_2 \right| \right|^{z_2}_{z_1} \quad (37)$$

265

$$\int \int \int_{v_j} \frac{\partial^2}{\partial z \partial z} \frac{1}{R_{2ij}} dv_j = \left| \left| -\tan^{-1} \left(\frac{xy}{z R_2} \right) \right| \right|^{x_2}_{x_1} \left| \left| y_2 \right| \right|^{z_2}_{z_1}, \quad (38)$$

where the variable z is given by equations 34 and 35.

The horizontal displacement field at the i th coordinates (x_i , y_i and z_i) due to the pressure change in the whole reservoir is
 calculated by

$$270 \quad \tilde{u}_{i_h} = \sqrt{\tilde{u}_{i_x}^2 + \tilde{u}_{i_y}^2} \quad (39)$$

where \tilde{u}_{i_x} and \tilde{u}_{i_y} are the x - and y - components of the displacement field at the i th coordinates given by equation 29, with
 $\alpha = x$ and y .

3.3 The discrete stress forward modeling due to a reservoir in a homogeneous elastic semi-infinite medium

By following the similar approach used in the displacement forward modeling due to a prism in a homogeneous elastic semi-infinite medium (subsection 3.2), the stress field of each prism assuming constant pressure is calculated by integrating over its volume the stress of a nucleus of strain located at its center. Next, the stresses due to a set of M prisms modeling the reservoir is summed to yield the stress field due to the pressure change in the whole reservoir.

Like equation 25, the stress field at the i th coordinates (x_i , y_i and z_i) due to the pressure change in the whole reservoir can be written as:

$$280 \quad \tilde{\sigma}_i(x_i, y_i, z_i) = \sum_{j=1}^M \int_{z_1}^{z_2} \int_{y_1}^{y_2} \int_{x_1}^{x_2} \boldsymbol{\sigma}_{1i} dx'_j dy'_j dz'_j + \int_{z_1}^{z_2} \int_{y_1}^{y_2} \int_{x_1}^{x_2} \boldsymbol{\sigma}_{2i} dx'_j dy'_j dz'_j, \quad (40)$$

where the limits of the integrals represent the borders of the j th prism modeling the reservoir in the following way: x_1 and x_2 are their south and north borders; y_1 and y_2 are their west and east borders; and z_1 and z_2 are their depths to the top and bottom.

From equations 21 and 22, we write, respectively, the α -component (where $\alpha = x$ and y) and the z -component of the stress field at the i th coordinates (x_i , y_i and z_i) due to the pressure change in the whole reservoir, i.e.:

$$\tilde{\sigma}_{i\alpha} = A \sum_{j=1}^M \Delta p_j \int_{v_j} \int \int \frac{\partial^2}{\partial \alpha \partial z} \frac{1}{R_{1ij}} dv_j + \int_{v_j} \int \int \frac{\partial^2}{\partial \alpha \partial z} \frac{1}{R_{2ij}} dv_j + 2 z_i \int_{v_j} \int \int \frac{\partial^3}{\partial \alpha \partial z^2} \frac{1}{R_{2ij}} dv_j, \quad (41)$$

and

$$\tilde{\sigma}_{iz} = A \sum_{j=1}^M \Delta p_j \int_{v_j} \int \int \frac{\partial^2}{\partial z^2} \frac{1}{R_{1ij}} dv_j - \int_{v_j} \int \int \frac{\partial^2}{\partial z^2} \frac{1}{R_{2ij}} dv_j + 2 z_i \int_{v_j} \int \int \frac{\partial^3}{\partial z^3} \frac{1}{R_{2ij}} dv_j, \quad (42)$$

where dv_j is the j th element of volume of the j th prism whose volume is v_j .

290 Like in the displacement field (equations 29 and 30), the three integrals, in the right-hand side of equations 41 and 42, are equal to quantities of the gravitational attraction produced by the j th prism considering that Δp_j is the density of the j th prism and the constants are equivalent to the gravitational constant. In equation 41, the first and second integrals correspond to the αz -component of the gravity gradient tensor (where $\alpha = x$ and y) produced, respectively, by the j th prism and j th image nucleus; and the third integral corresponds to the first derivative with respect to α of the zz -component of the gravity gradient tensor produced by the j th image nucleus. In equation 42, the first and second integrals correspond to the zz -component of the gravity gradient tensor produced, respectively, by the j th prism and j th image nucleus; and the third integral corresponds to the first derivative with respect to z of the zz -component of the gravity gradient tensor produced by the j th image nucleus.

Here, we also use the closed expressions of the gravitational potential and its derivatives produced by the 3D right rectangular prism derived by Nagy et al. (2000) and (2002) to calculate the stress field due to a volume source in a half-space. The first 300 integral in equations 41 and 42 corresponds, respectively, to the αz - and zz -components of the gravity gradient tensor produced by the j th prism modeling the reservoir. These second partial derivatives of $\frac{1}{R_{1ij}}$ with respect to xz , yz and zz are calculated using the analytical expressions given by equations 36 – 38 but substituting $\frac{1}{R_{2ij}} \equiv \frac{1}{R_2}$ by $\frac{1}{R_{1ij}} \equiv \frac{1}{R_1}$.

The second and third integrals in the right-hand side of equations 41 and 42 are related with the correction of the stresses considering a semi-space (image nucleus solution). These integrals depend on the distance R_{2ij} from the i th coordinate point of 305 the stress to the j th image nucleus, where the variable z is given by the equations 34 and 35. In the right-hand side of equations 41 and 42, the second integral is the second partial derivatives of $\frac{1}{R_{2ij}}$ with respect to xz , yz and zz given by equations 36 – 38 and the third integral is the third partial derivatives of $\frac{1}{R_{2ij}}$ with respect to xzz , yzz and zzz given by (Nagy et al. (2000)):

$$\int \int \int_{v_j} \frac{\partial^3}{\partial x \partial z^2} \frac{1}{R_{2ij}} dv_j = \left| \left| \left| -\frac{yz}{R_2} \left(\frac{1}{x^2 + z^2} \right) \right|_{x_1}^{x_2} \right|_{y_1}^{y_2} \right|_{z_1}^{z_2} \quad (43)$$

$$310 \quad \int \int \int_{v_j} \frac{\partial^2}{\partial y \partial z^2} \frac{1}{R_{2ij}} dv_j = \left| \left| \left| -\frac{xz}{R_2} \left(\frac{1}{y^2 + z^2} \right) \right|_{x_1}^{x_2} \right|_{y_1}^{y_2} \right|_{z_1}^{z_2} \quad (44)$$

$$\int \int \int_{v_j} \frac{\partial^3}{\partial z^3} \frac{1}{R_{2ij}} dv_j = \left| \left| \left| \frac{xy}{R_2} \left(\frac{1}{x^2 + z^2} + \frac{1}{y^2 + z^2} \right) \right|_{x_1}^{x_2} \right|_{y_1}^{y_2} \right|_{z_1}^{z_2} \quad (45)$$

3.4 Computation notes

In equations 31–33 and 36–33, we adopted the modifications proposed by Fukushima (2020). To overcome the zero division 315 in evaluating the arguments of the arctangent function, Fukushima (2020) replaced $\tan^{-1} \left(\frac{S}{T} \right)$ by

$$arctan2(S, T) = \begin{cases} atan(S/T) & \text{if } T \neq 0 \\ \pi/2 & \text{if } T = 0 \text{ and } S > 0 \\ -\pi/2 & \text{if } T = 0 \text{ and } S < 0 \\ 0 & \text{if } T = 0 \text{ and } S = 0 \end{cases} \quad (46)$$

If the argument of the logarithm is less than 10^{-10} , the logarithm is replaced by zero; otherwise the logarithm is calculated regularly

4 NUMERICAL APPLICATIONS

320 4.0.1 Disk-shaped reservoir under uniform depletion

Embedded in a semi-infinite homogenous medium, we simulated a vertical cylinder-like reservoir (Figure 2) with a radius of 500 m and whose horizontal coordinates of its center along the north-south and east-west directions are 0 m and 0 m, respectively. The depths to the top and to the bottom of the simulated reservoir are 750 m and 850 m, respectively. The reservoir is uniformly depleted by $\Delta p = -10$ MPa. The Young's modulus is 3300 (in MPa), the Poisson's coefficient is 0.25, 325 and the uniaxial compaction coefficient C_m (equation 10) is $2.2525 \cdot 10^{-4}$ MPa $^{-1}$.

To apply our methodology, we discretized the cylinder along the x - and y - directions into an 20×20 grid of prisms. Hence, we totalized 400 prisms all of them centered at 800 m deep, with depths to the top and to the bottom at 750 m and 850 m and with pressure contrast Δp_j , $j = 1, \dots, 400$ equal to -10 MPa. To apply the Geertsma's method (Geertsma, 1973), we used the disk-shaped reservoir described in Fjaer et al. (2008) with dimensions and physical properties defined above.

330 Figures 3 and 4 show cross-sections at $x = 0$ m of the displacement fields in 2D contour plots due to the pressure change in the whole cylindrical reservoir by using our methodology and Geertsma's method (Geertsma, 1973), respectively.

Because we defined the z -axis as positive downwards, the positive vertical displacement means a subsidence and the negative vertical displacement means an uplift. Figure 3 shows the horizontal and vertical displacements calculated, respectively, with equations 39 and 30 by our methodology that uses the closed expressions of the full integrations (equations 29 and 30) of 335 Nagy et al. (2000) and Nagy et al. (2002) (equations 31 – 38).

Figure 4 shows the radial and vertical displacements using Geertsma's method (Geertsma, 1973) considering an elastic homogeneous cylindrical reservoir under uniform depletion based on the nucleus-of-strain concept in the half-space, which in turn was proposed by Mindlin and Cheng (1950) and Sen (1951) in the theory of thermoelasticity.

In both cases (Figures 3b and 4b) the vertical displacements due to the entire the disc-shaped reservoir display a subsidence 340 (positive values) above the reservoir and an uplift (negative values) below the reservoir. We stress that the proposed volume integrations (equations 31 – 38) allowed to evaluate the vertical displacement (Figure 3b) throughout the entire reservoir including inside and outside the reservoir. Rather, the vertical displacement using Geertsma's method (Figure 4b) is only valid outside the reservoir.

The radial displacement using Geertsma's method (Figure 4a) shows positive values at the edges of the reservoir ($y = -500$ 345 and $y = 500$) with a singularity at the center of the reservoir ($x = 0$, $y = 0$ and $z = 800$ m). The horizontal displacement with the proposed full integration (Figures 3a) shows positive values at the edges of the reservoir ($y = -500$ and $y = 500$); however, it does not present sigularities inside the reservoir.

Figure 5 shows the x -component displacement and vertical displacement by our methodology that uses a full volume 350 integrations. These displacements are calculated along the x -axis, at $y = 0$ m and considering four surfaces located at the following depths: seafloor ($z = 0$ m), reservoir top ($z = 750$ m), reservoir center ($z = 800$ m) and reservoir bottom ($z = 850$ m). In the x -component of the displacement (Figure 5a), we can note an increased horizontal contraction from the center of the reservoir ($x = 0$) toward the reservoir edge ($x = 500$ m) where the maximum contraction of all surfaces occur. In the vertical displacement (Figure 5b), we can note a subsidence of the seafloor and the reservoir top (positive values) and an uplift of the reservoir bottom (negative values). The vertical displacements of the seafloor, the top and bottom of the reservoir for Geertsma's 355 method (Figure 6) show a similar behavior of those obtained by our methodology that uses a full volume integrations (Figure 5b). However, we note that the subsidence of the seafloor is more attenuated in the Geertsma's method than in our method. This fact is important because the moviment of the seafloor should be monitored in hydrocarbon fields under production.

Figure 7 shows the null stress through the free surface at the plane $z = 0$ m (equations 20 and 23) due to reservoir under uniform depletion.

360 **4.0.2 Disk-shaped reservoir under non uniform depletion**

Here, we kept the same dimensions of the cylindrical reservoir simulated previously. We also kept the reservoir properties, except the pressure. We simulated a non-uniform depletion scenario where the cylindrical reservoir is composed by two vertically juxtaposed cylinders, each one with a uniform depletion. The deepest cylinder is uniformly depleted by $\Delta p = -20$ MPa with its top and bottom at, respectively, 800 and 850 m deep. The shallowest cylinder is uniformly depleted by $\Delta p = -40$ MPa with its top and bottom at, respectively, 750 and 800 m deep.

365 We discretized the cylinders along the x –, y – and z – directions into an $20 \times 20 \times 2$ grid of prisms. This simulation totalized 800 prisms whose thicknesses are 50 m. The 400 deepest prisms are centered at 825 deep, with pressure contrast equal to -20 MPa and the 400 shallowest prisms are centered at 775 deep, with pressure contrast equal to -40 MPa

We calculate the displacement fields due to the pressure change in the whole cylindrical reservoir under non uniform depletion.

370 Figure 8 shows cross-sections at $x = 0$ m of the horizontal and vertical displacements, in 2D contour plots, calculated in the whole reservoir by using our methodology. Figure 9 shows the x –component displacement and vertical displacement that are calculated by our methodology along the x –axis, at $y = 0$ m and considering four surfaces located at the following depths: seafloor ($z = 0$ m), reservoir top ($z = 750$ m), reservoir center ($z = 800$ m) and reservoir bottom ($z = 850$ m).

375 By comparing Figure 8 with Figures 3, we can note similar behaviours of the displacement fields. However, the displacement fields of reservoir under non uniform depletion (Figure 8) attain higher values because the higher variation of the pressure in the whole cylindrical reservoir.

In general, the displacements on the seafloor, the top, the center and the bottom of the reservoir under non uniform depletion (Figure 9) show similar behaviors to the corresponding surfaces of the reservoir under uniform depletion (Figure 5). However,

380 we can note higher displacements of these surfaces in the reservoir under non uniform depletion (Figure 9) due to the higher variation of the pressure in the whole cylindrical reservoir. Moreover, we can observe that the x –component displacements (Figure 9a) produced by the top (black line) and the bottom (red line) of the reservoir under non uniform depletion are not coincident to each other and the vertical displacement on the center of the reservoir under non uniform depletion (blue line in (Figure 9b) varies along the x –axis. Finally, we stress that the subsidence on the seafloor due to the reservoir under non uniform depletion (green line in Figure 9b) attains higher values (close to 20 cm) than the subsidence of the seafloor due to the reservoir under uniform depletion (green line in Figure 5b).

385 We verify that the zero stress condition is satisfied at the free surface (equations 20 and 23) due to reservoir under a non uniform depletion as shown in Figure 10.

4.0.3 Reservoir with arbitrary geometry and under arbitrary pressure changes

In this numerical application, the reservoir model is a simplification of a realistic reservoir located in a production oil field in

390 offshore Brazil. The entire reservoir model comprises dimensions of 14 km in the north-axis, 13 km in the east-axis, and 0.6 km in the down-axis. The depths to the top and bottom of the reservoir model are 2,712 m and 3,312 m, respectively. The components of the displacements are calculated at 0 m deep, on a regular grid of 100×80 observation points along the north-

and east-directions, respectively. We discretized the reservoir along the x –, y – and z – directions into an $14 \times 13 \times 2$ grid of prisms. The Young’s modulus is 3300 (in MPa), the Poisson’s coefficient is 0.25, and the uniaxial compaction coefficient C_m (equation 10) is $2.2525 \cdot 10^{-4}$ MPa $^{-1}$. In the 3D perspective view of the pore pressure distribution of the simulated reservoir shown in Figure 11, we can see that the pressures vary from 0 to -0.72 MPa. Figure 12 shows cross-sections at $x = 8$ km of the horizontal and vertical displacements, in 2D contour plots, calculated in the whole reservoir by using our methodology. Figure 13 shows the null stress through the free surface (equations 20 and 23) due to reservoir with arbitrary geometry and under arbitrary pressure distribution.

400 5 Conclusions

Grounded on the similarity between the gravitational potential produced by a volume source under a density variation and the displacement field produced by a volume source in a half-space under a pressure variation, we have presented the analytical solution for the displacement field due to reservoir compaction with arbitrary geometry and under non-uniform pressure distribution. Our approach calculates the displacement field due to a reservoir by approximating its 3D pressure distribution through a piecewise constant function defined on a user-specified grid of 3D vertical prisms juxtaposed in the x –, y – and z – directions. By using the nucleus of strain as an infinitesimal volume element for each prism, we have calculated the displacement solution yielded by each prism through a 3D integration over the prism volume. The sum of the displacements produced by the prisms is the final displacement field due to the whole reservoir. The adopted exact analytical formulae, based on the gravitational field, to carry out the full integrations and calculate the displacement field due to reservoir compaction are valid expressions either outside or inside the prisms because the implemented expressions make use of modified arctangent function. We have demonstrated the use of these exact analytical expressions by applying them to calculate the displacement fields due to cylindrical reservoirs with uniform and non-uniform pressure distributions and to realistic reservoir model of a production oil field in offshore Brazil with arbitrary geometry and under arbitrary pressure distribution. All the numerical applications produced null stress fields at the free surface showing that the condition of null tractions at the free surface has been met. We have presented routines written in Python language (Python 3.7.6) to calculate the displacement and stress fields due to a reservoir with arbitrary shape and non-uniform distribution of pressure changes. The numerical applications and figures showing the results in this article were produced in Jupyter Notebook.

Code and data availability. The current version of our code is freely distributed under the BSD 3-clause licence and it is available for download at Zenodo: <http://doi.org/XXXXXXXX>. The latest development version of our code can be freely downloaded from a repository on GitHub (<https://github.com/pinga-lab/reservoir-compaction>). Instructions for running the current version of our code are also provided on the repository. The code is still being improved and we encourage the user to work with the latest development version. The code was developed as an open-source Python language (Python 3.7.6). The numerical applications were produced in Jupyter Notebook. The data of the pore pressure distribution simulating a realistic reservoir (*realistic – model.pickle*) are available in the above-mentioned repositories.

Author contributions. VCFB and VCOJr deduced the equations in this paper. VCFB and ADA implemented the numerical applications

425 presented in this paper. Most of the python codes were developed by VCOJr with some participation of VCFB. All authors contributed to the writing of the paper.

Competing interests. The authors declare that they have no conflict of interest.

Acknowledgements. Andre D. Areclaro thanks Petrobras, especially, the Multiphysics Group. Valeria C.F. Barbosa was supported by fellow-

ships from: CNPq (grant 307135/2014- 4) and FAPERJ (grant E-26/202.582/2019). Vanderlei C. Oliveira Jr. was supported by fellowships

430 from: CNPq (grant 308945/2017-4) and FAPERJ (grant E-26/202.729/2018).

Financial support. This work is supported by the Brazilian research agencies Conselho Nacional de Desenvolvimento Científico e Tec-

nológico (CNPq) and Fundação Carlos Chagas Filho de Amparo à Pesquisa do Estado do Rio de Janeiro (FAPERJ).

References

- Beltrami, E.: Opere Matematiche, Hoepli, Milano, 1902–1920.
- 435 Borges, F., Landro M., and Duffaut, K.: Time-lapse seismic analysis of overburden water injection at the Ekofisk field, southern North Sea, GEOPHYSICS, 85, B9–B21, 2020
- Dahm, T., Cesca, S., Hainzl, S., Braun, T., and Krüger, F.: Discrimination between induced, triggered, and natural earthquakes close to hydrocarbon reservoirs: A probabilistic approach based on the modeling of depletion-induced stress changes and seismological source parameters, J. Geophys. Res. Solid Earth, 120, 2491–2509, 2015.
- 440 Faer, E., Holt, R. M., Horsrud, P., Raaen, A.M., and Risnes, R.: Petroleum related rock mechanics: Elsevier, 53, 2008.
- Fukushima, T.: Speed and accuracy improvements in standard algorithm for prismatic gravitational field, Geophys. J. Int., 222, 1898–1908, 2020.
- Geertsma, J.: A remark on the analogy between thermoelasticity and the elasticity of saturated porous media. J. Mech. Phys. Solids, 6, 13–16, 1957
- 445 Geertsma, J.: Problems of rock mechanics in petroleum production engineering, in: Proc. First Cong. Int. Soc. Rock Mech., 1, 585–594, 1966.
- Geertsma, J.: Land Subsidence above compacting oil and gas reservoirs, J. Pet. Tech. 25, 734–744, 1973.
- Geertsma, J., and van Opstal, G.: A numerical technique for predicting subsidence above compacting reservoirs, based on the nucleus of strain concept," Verhandelingen Kon. Ned. Geol. Mijnbouwk., 28, 63–78, 1973.
- 450 Goodier, J. N.: On the Integration of the Thermo-elasti equations, Phil. Mag. 7, 1017-1032, 1937.
- Grigoli, F., Cesca, S., Priolo, E., Rinaldi, A.P., Clinton, J.F., Stabile, T.A., Dost, B., Fernandez, M.G., Wiemer, S. and, Dahm T.: Current challenges in monitoring, discrimination, and management of induced seismicity related to underground industrial activities: a European perspective, Rev. Geophys., 55, 310–340, 2017
- Kellogg, O. D.: Foundations of Potential Theory, rederick Ungar Publishing Company, 1929.
- 455 Mehrabian, A., and Abousleiman, Y.A.: Geertsma's subsidence solution extended to layered stratigraphy, J. Pet. Sci. Eng., 130, 68–76, 2015.
- Mindlin, R.D. and Cheng, D.H.: Thermoelastic stress in the semi-infinite solid, J. Appl. Phys. 21, 931–933, 1950.
- Muñoz, L.F.P. and Roehl, D: An analytical solution for displacements due to reservoir compaction under arbitrary pressure changes, Appl. Math. Modell., 52, 145–159, 2017.
- Nagy, D., Papp, G., and Benedek, J.: The gravitational potential and its derivatives for the prism: Journal of Geodesy, 74, 552–560, 2000.
- 460 Nagy, D., Papp, G., and Benedek, J.: Corrections to "The gravitational potential and its derivatives for the prism": Journal of Geodesy, 76, 475, 2002.
- Segall, P.: Induced stresses due to fluid extraction from axisymmetric reservoirs. Pure Appl. Phys. 139, 536–560, 1992.
- Sen, B.: Note on the Stresses Produced by Nuclei of Thermoelastic Strain in a Semi-infinite Solid, Quart. Appl. Math., 8, 365–369, 1951.
- Sharma, B.D.: Stresses in an infinite slab due to a nucleus of thermoelastic strain in it, Z. Angew. Math. Mech., 36, 565–589, 1956.
- 465 Tao, L.N: Integration of the dynamic thermoelastic equations, Int. J. Eng. Sci., 9, 489–505, 1971
- Tempone, P., Fjaer, E., and Landro, M.: Improved solution of displacements due to a compacting reservoir over a rigid basement, Appl. Math. Modell. 34, 3352–3362, 2010.
- Tempone, P., Landro, M., and Fjaer, E.: 4D gravity response of compacting reservoirs: Analytical approach, Geophysics, 77, G45–G54, 2012.

van Thienen-Visser, K. and Fokker, P. A.:The future of subsidence modelling: compaction and subsidence due to gas depletion of the

470 Groningen gas field in the Netherlands, 96, Netherlands Journal of Geosciences, 96, s105–s116, 2017.

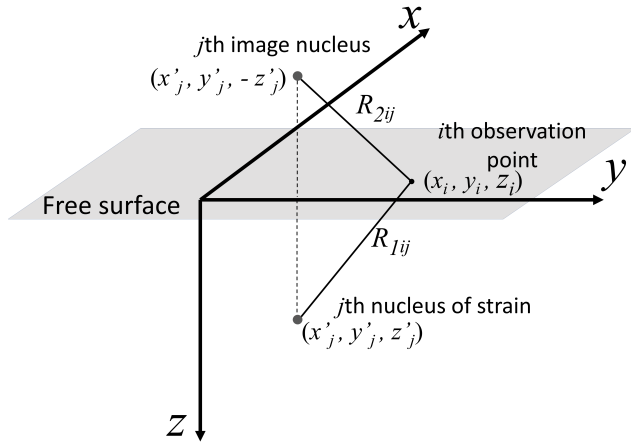


Figure 1. Schematic representation of the geometry of the nucleus of strain in a semi-infinite medium. After Muñoz and Roehl (2017). The adopted Cartesian coordinate system considered the x -axis pointing to north, the y -axis pointing to east and the z -axis pointing downward.

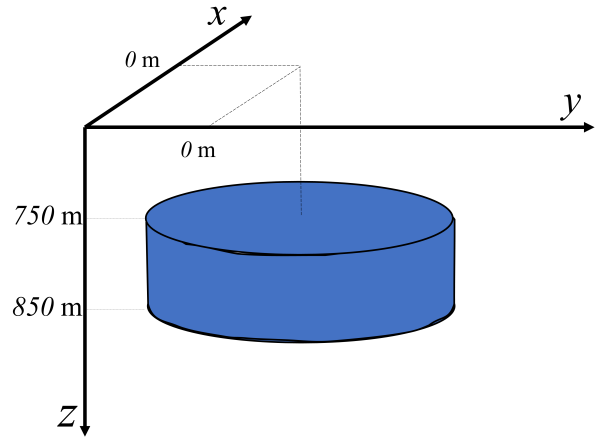


Figure 2. Disk-shaped reservoir under uniform depletion with a radius of 500 m

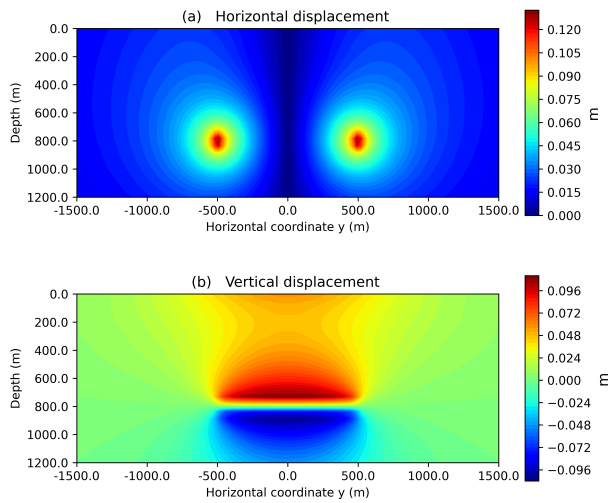


Figure 3. Reservoir under uniform depletion: (a) Horizontal displacement (equation 39) and (b) vertical displacement (equation 30) by our methodology that uses the closed expressions of the volume integrations given by Nagy et al. (2000) and Nagy et al. (2002) (equations 31-38)

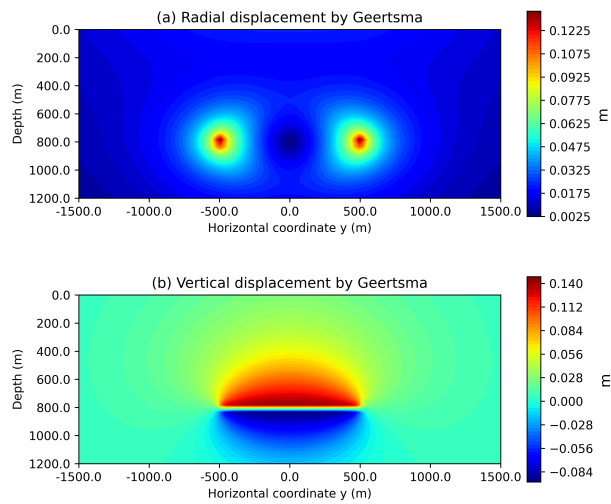


Figure 4. Reservoir under uniform depletion: (a) Radial displacement and (b) vertical displacement using Geertsma's method (Geertsma, 1973) considering an elastic homogeneous cylindrical reservoir under uniform depletion (Fjaer et al., 2008)

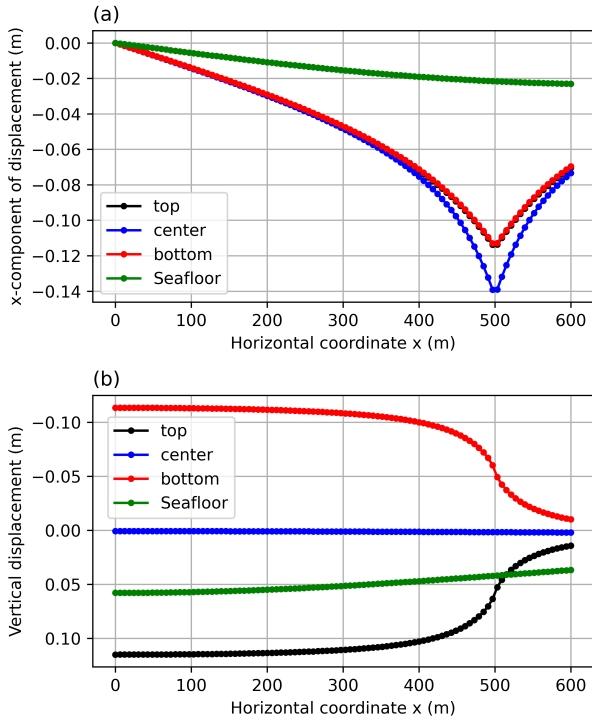


Figure 5. Reservoir under uniform depletion: (a) Horizontal x-component displacement and (b) vertical displacement by our methodology that uses the closed expressions of the volume integrations given by Nagy et al. (2000) and Nagy et al. (2002) (equations 31-38). These displacements are calculated along the x-axis, at $y = 0$ m and z located at the depths of: seafloor ($z = 0$ m), reservoir top ($z = 750$ m), reservoir center ($z = 800$ m) and reservoir bottom ($z = 850$ m).

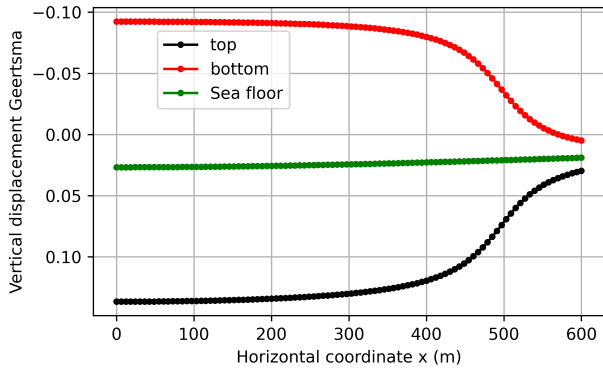


Figure 6. Reservoir under uniform depletion: Vertical displacement using Geertsma's method (Geertsma, 1973) considering an elastic homogeneous cylindrical reservoir under uniform depletion (Fjaer et al., 2008). The displacement is calculated along the x-axis, at $y = 0$ m and z located at the depths of: seafloor ($z = 0$ m), reservoir top ($z = 750$ m), and reservoir bottom ($z = 850$ m).

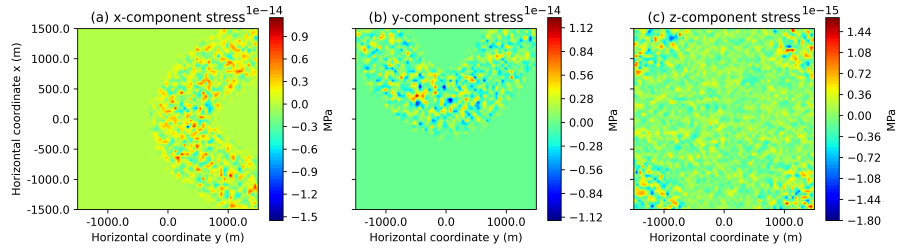


Figure 7. Reservoir under uniform depletion: (a) x –, (b) y –, and (c) z – components of the stress at the free surface.

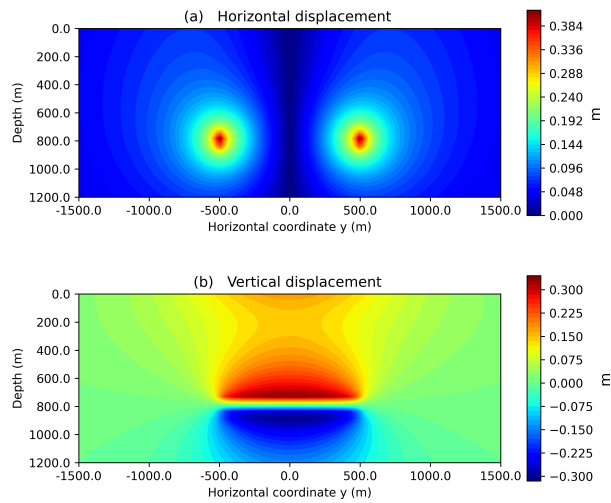


Figure 8. Reservoir under non uniform depletion: (a) Horizontal displacement (equation 39) and (b) vertical displacement (equation 30) by our methodology that uses the closed expressions of the volume integrations given by Nagy et al. (2000) and Nagy et al. (2002) (equations 31-38)

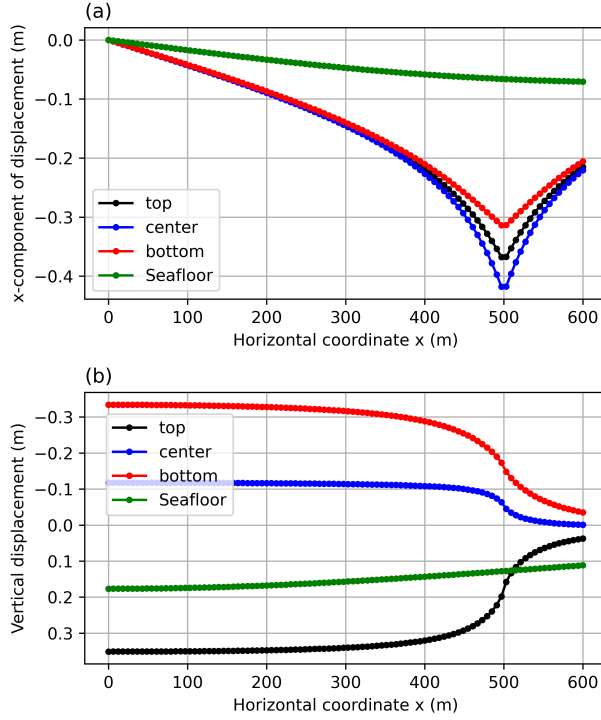


Figure 9. Reservoir under non uniform depletion: (a) Horizontal x-component displacement and (b) vertical displacement by our methodology that uses the closed expressions of the volume integrations given by Nagy et al. (2000) and Nagy et al. (2002) (equations 31-38). These displacements are calculated along the x-axis, at $y = 0$ m and z located at the depths of: seafloor ($z = 0$ m), reservoir top ($z = 750$ m), reservoir center ($z = 800$ m) and reservoir bottom ($z = 850$ m).

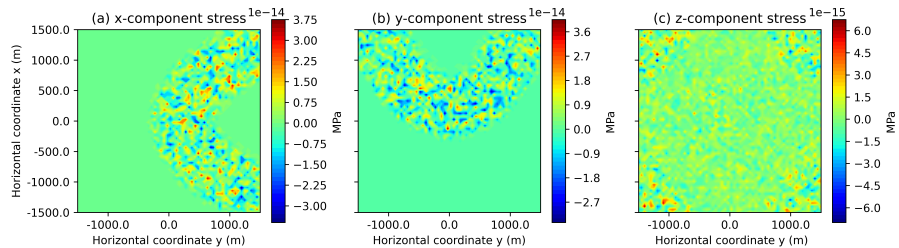


Figure 10. Reservoir under non uniform depletion: (a) $x-$, (b) $y-$, and (c) $z-$ components of the stress at the free surface.

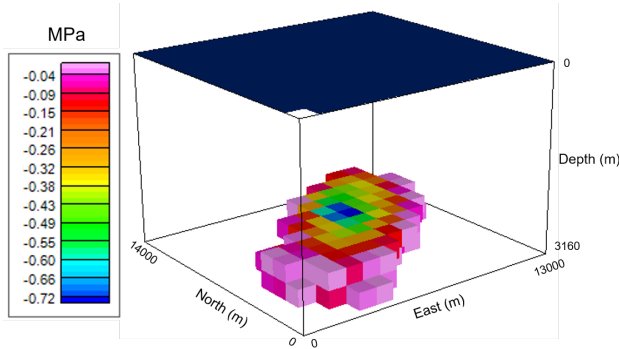


Figure 11. Reservoir with arbitrary geometry and under arbitrary pressure changes: 3D perspective view of the pore pressure distribution of a realistic reservoir located in a production oil field in offshore Brazil.

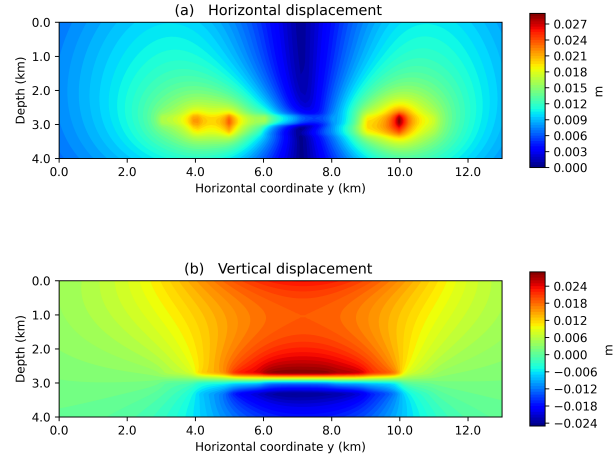


Figure 12. Reservoir with arbitrary geometry and under arbitrary pressure changes: (a) Horizontal displacement (equation 39) and (b) vertical displacement (equation 30) by our methodology that uses the closed expressions of the volume integrations given by Nagy et al. (2000) and Nagy et al. (2002) (equations 31-38)

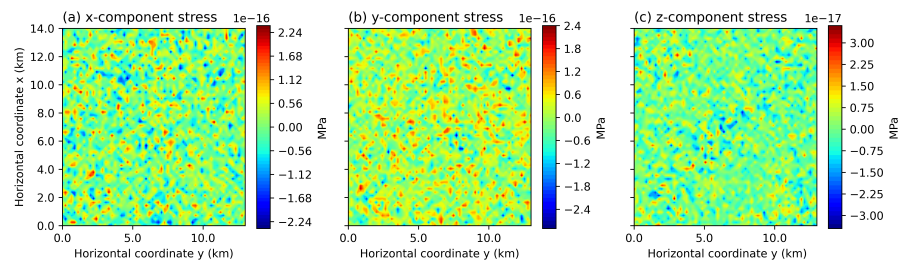


Figure 13. Reservoir with arbitrary geometry and under arbitrary pressure changes: (a) x –, (b) y –, and (c) z – components of the stress at the free surface.